



A Novel Exact Solution of Longshore Current and Its Application on Permeable Groin

Hasdinar Umar ^{1*}, Fuad M. Assidiq ¹, Radianta Triatmadja ², Achmad Y. Baeda ¹

¹ Department of Ocean Engineering, Universitas Hasanuddin, Gowa, 92171, Indonesia.

² Department of Civil and Environmental Engineering, Universitas Gadjah Mada, Yogyakarta, 55281, Indonesia.

Received 22 July 2024; Revised 09 January 2025; Accepted 14 January 2025; Published 01 February 2025

Abstract

One major environmental problem exacerbated by longshore currents is beach erosion. Groins are a common defense tactic built perpendicular to the shore. However, conventional impermeable groins promote downstream erosion and disrupt sediment movement. Permeable groins provide a more environmentally friendly option, allowing some sediment to flow through. This study examines the effects of permeable groins on longshore currents. Permeable groins are not included in currently used longshore current equations. This study fills this gap by creating a new longshore current velocity equation considering permeable groins. The longshore current equation with the groin was developed based on the momentum equation in the longshore direction without the influence of lateral mixing and the assumption that base friction will rise due to the groin. Therefore, it was determined that the base shear stress after the groin was equal to the base shear stress plus the drag caused by the groin. The result shows that the longshore current equation through the groin is a function of the breaking wave parameter and the resistance parameter owing to the groin. Longshore current velocities with and without permeable groins of different densities were measured in wave basins. We collected information on groin characteristics, current velocities, and breaking wave heights. This investigation validates the shortcomings of the current equations.

Keywords: Friction Coefficient; Groin Density; Longshore Current; Permeable Groin.

1. Introduction

Coastal erosion, a significant and urgent environmental issue in coastal areas, is influenced by various factors [1-3]. Longshore currents have been identified as a major contributor to erosion in these regions, supported by multiple research studies [4-7]. In Serangai Village, for instance, the impact of longshore currents on coastal erosion is evident in the gradual retreat of the shoreline, leading to the loss of valuable land and infrastructure [8]. Similarly, in Kragan Village, the relentless action of longshore currents has resulted in the disappearance of once-thriving beaches, posing a threat to the local tourism industry [9]. Additionally, local human activities, such as sand mining and coral reef destruction, exacerbate coastal erosion and compromise natural protective barriers. A case study on Kragan Village beaches reveals concerning patterns of coastal land loss, emphasizing the urgent need for sustainable coastal management strategies to protect vulnerable areas. The urgency of the situation calls for immediate action, making the findings of this study all the more relevant and significant. As vital coastal structures, groins are crucial in controlling sediment movement, preventing erosion, and stabilizing shorelines. By redirecting sediment flow and halting longshore sediment transport, they act as a formidable defense against erosion and protect coastlines [10]. Research has consistently demonstrated the effectiveness of impermeable groins in reducing sediment transport and longshore currents, as evidenced in Richards Bay port using GENESIS software [11]. The proper placement and diligent monitoring of groins are key to long-term coastal conservation and global management plans [12].

* Corresponding author: hasdinar.umar@gmail.com

 <http://dx.doi.org/10.28991/CEJ-2025-011-02-07>



© 2025 by the authors. Licensee C.E.J, Tehran, Iran. This article is an open access article distributed under the terms and conditions of the Creative Commons Attribution (CC-BY) license (<http://creativecommons.org/licenses/by/4.0/>).

Adopting a high, long, impermeable groin construction that spans the breadth of the wave zone in the updrift groin effectively halted sediment movement along the coast, aiming to contain beach erosion in the immediate construction area. However, this rigid approach inadvertently caused a sediment deficit in the downdrift groin, where erosion persisted despite the continuing movement of sediment, resulting in significant changes along the coastline [11, 13]. Implementing a permeable groin structure is a more sustainable solution to address the sediment discrepancy and erosion issue. Unlike impermeable groins, which disrupt the natural flow of sediment, a permeable groin features openings that facilitate the passage of currents [14]. By allowing sediment to flow through, a permeable groin enables sediment transfer towards the downdrift groin, mitigating erosion and maintaining the coastal equilibrium [15, 16]. The effectiveness of a permeable groin structure hinges on various factors, notably the size and density of the gaps within the groin. These openings serve as conduits for maintaining the longshore current, which is crucial in transporting sediment along the coastline. Adjusting the density and size of the gaps within the permeable groin influences not only the magnitude of the longshore current but also the efficiency of sediment transport. Consequently, a well-designed permeable groin can effectively address the sediment imbalance between the updrift and downdrift areas, fostering a more sustainable coastal environment [17, 18].

Pile groins impact coastal sediment dynamics by obstructing sediment flow and supplying downstream groins with essential deposits. In Northwestern Egypt, permeable groins caused extensive erosion along an 1100-meter shoreline stretch west of Alexandria [19]. Factors like groin length, spacing, and density influence the relationship between groins and environmental variables. Permeable groins reduce current speed without completely stopping movement, affecting coastal hydrodynamics. A mathematical model by Pranata and collaborators shows how groin length and spacing impact current velocities. Study results show a significant decrease in current speed with double permeable groins, reducing speeds by 59.21% to 80.49% for different lengths. This highlights the effectiveness of permeable groins in managing coastal currents and their implications for coastal management strategies. Impermeable groins significantly reduced longshore current velocity by 57.42% to 89.91%, depending on groin length. A key finding was the negative correlation between the groin length-to-spacing ratio and current velocity reduction, indicating that a lower ratio improves efficacy in coastal engineering.

In this extensive investigation, our primary objective will be to thoroughly explore the application of equations in evaluating and examining the magnitude of longshore currents after implementing a pile groin structure. It is crucial to highlight that groins have conventionally served as a strategic approach to regulate and manage the behavior of longshore currents along coastlines. Historically, the development of equations governing coastal currents has predominantly relied on practical observations, thus heavily depending on empirical data. Notably, the groundbreaking research conducted by Longuet-Higgins [20] has significantly advanced the comprehension of longshore currents by introducing the concept of radiation stress. This innovative theory elucidates that waves induce an additional flow of momentum, ultimately influencing the formation and behavior of longshore currents. Specifically, as waves approach the shore and transport water masses and momentum in a defined direction, they trigger the creation of currents that run parallel to the coastline, further shaping the dynamics of coastal environments.

In this study, we will explore how the equations may be used to analyze the size of the longshore currents following the existence of a pile groin structure. As previously described, groins were employed to control the longshore currents. Since equations for coastal currents were typically only created based on observations, they were solely reliant on empirical data. Longuet-Higgins & Stewart [21] proposed radiation stress, which they utilized to describe longshore currents. Radiation stress is the excess flow of momentum caused by the presence of waves. Waves approaching the beach and carrying water masses and momentum in that direction cause currents to form along the coast. Offshore, surf and swash zones are where waves propagate as they get closer to the shoreline. Triatmodjo [22] explained that of the three regions, the surf zone and swash zone wave characteristics were the most crucial for the research of coastal dynamics.

The theory of the equation of the longshore current was created by Longuet-Higgins [20] by taking into account a straight and flat beach with a beach depth (h) as a function of the distance to the coastline (x) and the perpendicular distance to the shoreline ($x = 0$). The longshore current equation with a groin structure was developed using the momentum equation in the longshore direction without lateral mixing, assuming that a permeable pile groin construction enhanced the bottom friction. The fundamental shear stress after the permeable groin structure (pile groin) was considered equal to the fundamental shear stress plus the drag factor/friction by the permeable groin structure [20]. The direction of wave propagation towards Semarang waters will undergo refraction and shoaling due to variations in depth, according to studies of coastal currents caused by wave transformation in Semarang waters. According to height measurement and significant wave period, the longshore current velocity is 1.586 m/s, although the modeling results show a range of 0.9017 to 1.1832 m/s [23].

The paper is structured methodically, beginning with a brief overview of relevant literature on longshore current and permeable groin in Section 2. Following this, Section 3 outlines the experimental measurements conducted. In Section 4, the paper delves into the analysis of longshore current distributions, the introduction of a novel model for longshore current under a permeable groin, and the verification of this new model. Finally, Section 5 offers an elaborate summary of the main findings derived from the research.

2. Background

Modern theories of longshore currents first emerged due to significant developments in the late 1960s and early 1970s, notably stemming from the introduction of the concept of radiation stress. These theories comprehensively explain how waves approaching the shore at specific angles generate a momentum flux that aligns along the shoreline. This gradient in momentum flux serves as a crucial driving force behind forming longshore currents. Among the prominent contributors to these theories are Longuet-Higgins [20], Komar & Inman [24], and Larson & Kraus [25], whose approaches have been widely adopted in coastal studies. Each approach offers unique insights into the mechanisms governing longshore currents, enhancing our understanding of coastal dynamics. In the subsequent subsection, we delve into the key characteristics and fundamental principles underpinning these seminal theories to provide a comprehensive overview of their implications and applications in coastal engineering and oceanography.

In 1970, Longuet-Higgins [20] significantly contributed to the field by introducing a comprehensive theory on the longshore current equation. Specifically, his work focused on an in-depth analysis of shoreline dynamics, particularly when considering a beach with specific characteristics, such as straight and flat. He delved into the complex relationship between beach depth and its variations concerning the distance from the shoreline and the distance perpendicular to it. Longuet-Higgins' research established two fundamental equations, Equations 1 and 2, which encapsulate the essence of the longshore current phenomenon. These equations highlight the interplay between various factors affecting the current, shedding light on the importance of lateral mixing parameters in defining and understanding this intricate natural process.

$$\langle v \rangle = \frac{5\pi}{8C_f} u_m (\tan \beta \tan \alpha) \quad (1)$$

where $\langle v \rangle$ is longshore current (m/s), π is radian (3.14), C_f is friction coefficient, u_m is orbital velocity (m/s), $\tan \beta$ is beach slope, α is wave angle ($^\circ$).

$$\langle v \rangle = \left(\frac{h}{h_b} \right) \times \begin{cases} v_b & h < h_b \\ 0 & h > h_b \end{cases} \quad (2)$$

with

$$v_b = \frac{5\pi \tan \beta}{16 C_f} \gamma_b \sqrt{g h_b} \sin \alpha_b \quad (3)$$

where v_b is longshore current (m/s), π is radian (3.14), C_f is friction coefficient, $\tan \beta$ is beach slope, γ_b is breaking wave parameter, g is gravity acceleration (m/s^2), h_b is breaking wave height (m), α_b is breaking wave angle ($^\circ$)

Komar & Inman [24] is a notable figure in coastal research who formulated a theory regarding the longshore current and conducted a thorough analysis using field data to support his findings. This research unveiled a significant trend indicating that $\tan \beta C_f^{-1}$, a mathematical term representing a specific angle in his analysis, remained relatively constant. By leveraging this constant factor, Equation 4 accurately depicts the velocity of the longshore current.

$$\langle v \rangle = 2.7 u_m \sin \alpha_b \cos \alpha_b \quad (4)$$

where $\langle v \rangle$ is longshore current (m/s), u_m is orbital velocity (m/s), α_b is breaking wave angle ($^\circ$)

Larson & Kraus [25] derived the longshore current equation by using the linear wave theory under shallow water conditions and by considering the equilibrium of the beach profile. This mathematical relationship is linked to Equation 5, providing a fundamental understanding of the dynamics of longshore currents in coastal environments. They developed a model that captures the intricate sediment transport processes along shorelines by incorporating the complex interplay between wave behavior and beach morphology.

$$\langle v \rangle = \frac{5}{24} \frac{\pi \gamma_b \sqrt{g}}{C_f} A^2 \frac{x^{1/3}}{\sqrt{d_b}} \sin 2\alpha_b \quad (5)$$

where $\langle v \rangle$ is longshore current (m/s), π is radian (3.14), C_f is friction coefficient, γ_b is breaking wave parameter, g is gravity acceleration (m/s^2), d_b is breaking wave depth (m), α_b is breaking wave angle ($^\circ$)

The average speed of longshore currents under non-sinusoidal wave conditions is as follows.

$$\langle v \rangle = \frac{\frac{5}{8} H_b \sqrt{\frac{g}{h_b}} (\tan \beta \sin \alpha_b)}{\left(\frac{2+\gamma}{4} \right) C_f} \quad (6)$$

where $\tan \beta$ is the slope of the coast, H_b is the breaking wave height (m), α_b is the breaking wave angle, γ is the ratio between the breaking wave height (H_b) and the breaking wave depth (h_b), and h_b is the breaking wave depth (m).

Research on pile permeable groins is noticeably lacking in the current body of literature. The available research findings fall short in terms of providing a comprehensive framework that can be reliably applied in the design of pile-permeable groin structures. As a result, the focus of this study revolves around formulating an equation that accurately represents the behavior of longshore currents following the installation of a pile-permeable groin. This equation development aims to build upon the foundational work of Longuet-Higgins [20], a seminal study that delves into the intricate dynamics of the surf zone phenomenon. By refining and enhancing the existing knowledge base with a specialized focus on Longuet-Higgins' insights, this research endeavors to fill the significant gaps in understanding the impact of pile permeable groins on longshore currents and coastal processes. Through rigorous exploration of these interconnected elements, this study aims to contribute valuable insights to inform the effective design and implementation of pile-permeable groin structures in coastal engineering practices.

3. Research Methodology

3.1. Research Flow Framework

The research flow framework, starting from the preparation stage to data analysis until completion, can be seen in Figure 1.

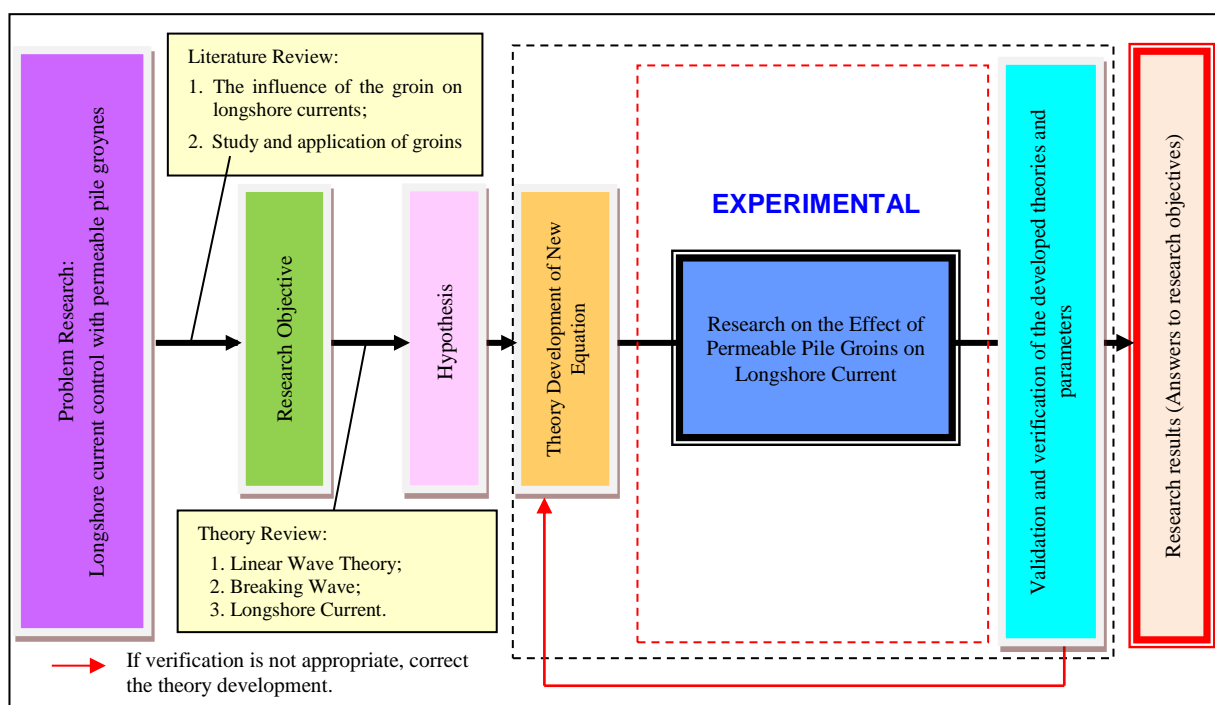


Figure 1. Flow Framework of The Study

3.2. Experimental Settings

The experiments were conducted in a three-dimensional wave basin at the Hydraulics Laboratory, Civil and Environmental Engineering, Universitas Gadjah Mada, Indonesia. The wave basin is 20 meters in length, 10 meters in width, and one meter deep.

This enabled more realistic flow and wave conditions on the beach to be simulated than those produced by a two-dimensional model. The effect of permeable groin structure parameters could be observed in greater detail and more comprehensively. The magnitude of the longshore current could also be measured more accurately. In parallel with the fixed-bed beach model (FBM), the permeable groin model (PGM) was constructed by the design specifications outlined in Figure 1, wherein the topographic form was calculated using Manning's equation of $n = 0.012$. Furthermore, the FBM and PGM and their respective instrumentation were placed according to the design above.

Once the groin model and measuring instruments were positioned as specified, observations and measurements were made regarding the influential parameters. It is theorized that the parameters of breaking wave height H_b and breaking wave angle α_b are essential for determining the magnitude of the longshore current v . Therefore, changes observed in these parameters after the presence of permeable groin structures will be documented in this research phase. In addition to the current parameters, this research phase also examines the structural parameters of the permeable groin, namely the diameter of the pile d_t and the distance between the piles a , as these parameters also affect the magnitude of the longshore current along the groin. These parameters are presented in Table 1 and Figures 2 and 3.

Table 1. Permeable variations on the groin structure model

Model	Diameter d_t (cm)	Distance between piles a (cm)
M2	1.50	0.7
M3	1.50	0.7
M4	1.25	0.7
M5	1.25	0.7
M6	1.50	1.0
M7	1.50	1.0
M8	1.25	1.0
M9	1.25	1.0

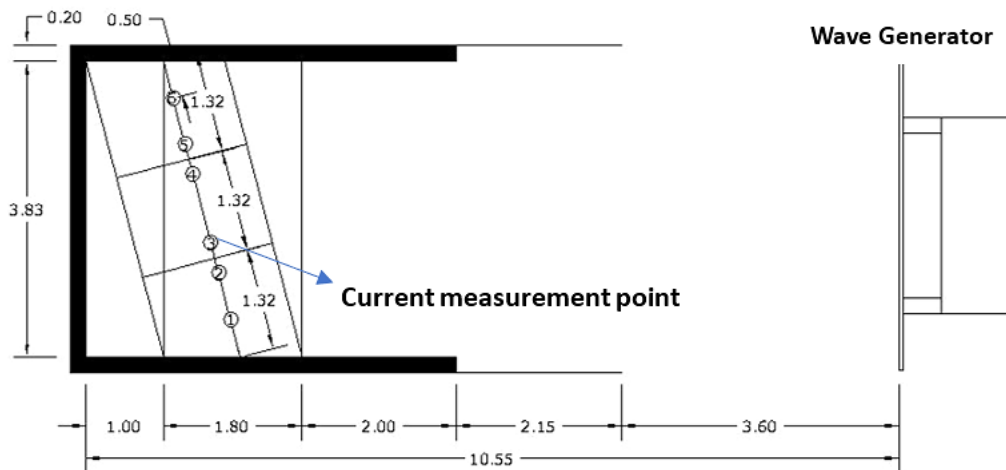


Figure 2. Top view of fixed-bed beach model and measurement points



Figure 3. Sample groin structure model; (a) Model M1 (impermeable), (b) Model M2, and (c) Model M9

3.3. Longshore Current Measurement Procedures

Longshore current measurements will be performed using the Acoustic Doppler Velocity (ADV) tool, with measurement points in Figure 2. Due to the limited water depth in the coastal model, it is essential to note that current measurements using ADV in the research model can only be performed at a single depth point for each measurement location. A minimum distance of 5 cm must be maintained between the probe tip and the ocean floor for current measurements to be conducted using the ADV tool. However, the sensor can be reflected perfectly at depths above 5 cm, allowing for accurate measurements even when close to the ocean floor. In contrast, the depth in the surf zone, particularly in the area after wave breaking, is less than 5 cm.

A more effective approach to measuring currents along the coast is the floating object method. This method utilizes float balls, which are deployed with a throwing device, to ascertain the average velocity of the current over a given area. The motion of the float ball is recorded via video camera, and its position is digitally captured using in-house code written in Visual Basic. Figure 4 visually represents the floating object's movement in the surf zone.

The float balls utilized as floating objects have a radius of 1.7 cm, a volume of 20.6 cm³, and a mass of 2.3 grams. To achieve an optimal current movement, the specific gravity of the ball must be as close as possible to the specific gravity of water, which is 1 gram/cm³. Consequently, the floats are filled with water until their weight reaches 20.6 grams, ensuring their particular gravity is consistent. After achieving an appropriate density for digitization purposes, float coloration facilitates the floats' x- and y-axis positioning.

The float ball's movement is digitized through the Track object program with a video recording speed of 30 frames per second. Before being processed in the Track Object Program, the video of the movement of the float balls was split into still frames using the Ulead Video Studio Program. The x -and- y -positional data of the buoy balls throughout a single wave period was obtained from the Track Object Program. Subsequently, the positional data, expressed initially in pixel units, was converted into centimeters for analysis. The conversion from pixels to centimeters is achieved by measuring the distance between the positions of the 1st ball and the 10th ball, which is 40 cm in this case, as presented in Figure 4. The exact distance in pixels was quantified through the Track above Object Program, and an outcome of 80.8 pixels was yielded. Consequently, one centimeter is equivalent to two pixels, with one pixel representing two-point-zero-two centimeters.

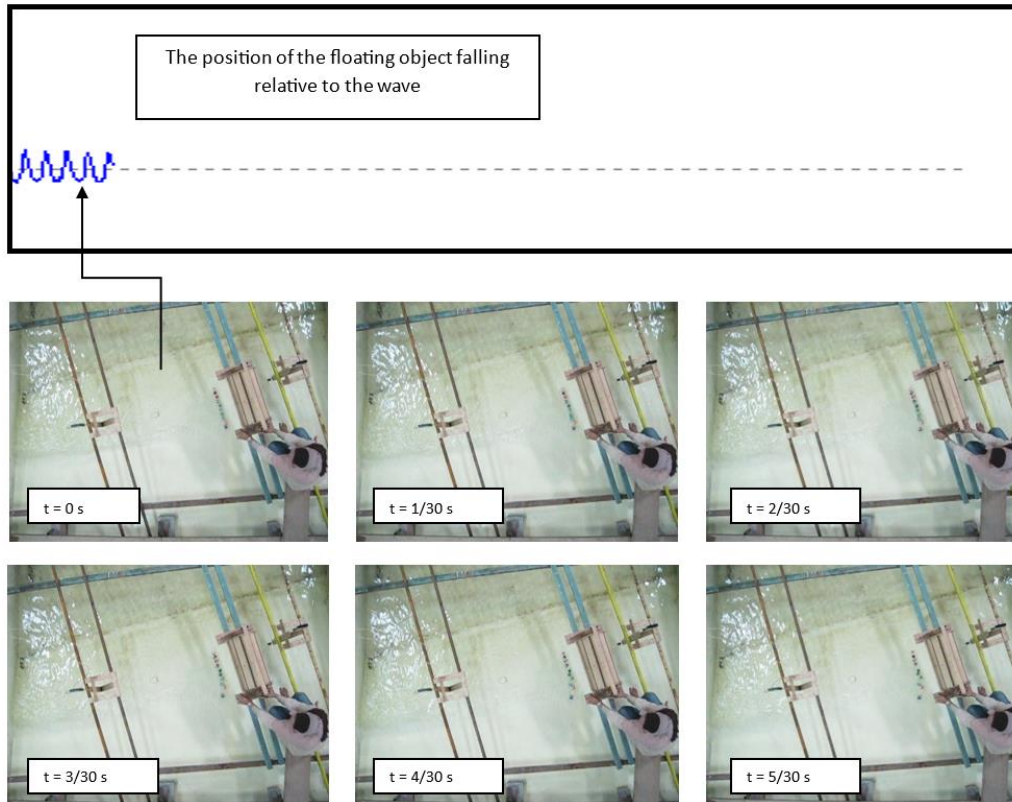


Figure 4. Floating objects moving under no groin structure

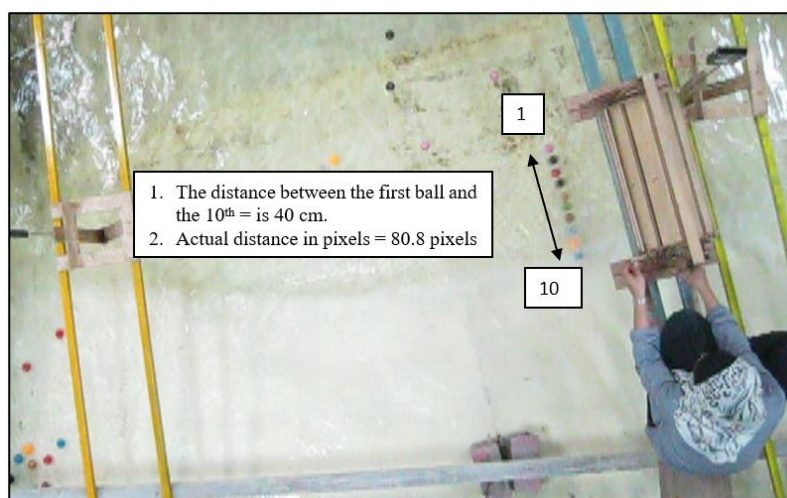


Figure 5. The distance between the first ball and the tenth ball

The current speed of the measurement results at the shoreline position ($x = 0$) is theoretically zero. The measurement data is the average alongshore current speed data using buoy balls. The results of current measurements using buoy balls in conditions with groins also show that the speed on the shoreline is never zero; this is caused by the influence of the uprush, which pushes the buoy balls relatively far so that the measured speed is not zero and is even relatively large. However, the current speed in the surf zone is relatively close to the theoretical line (see Figure 6).

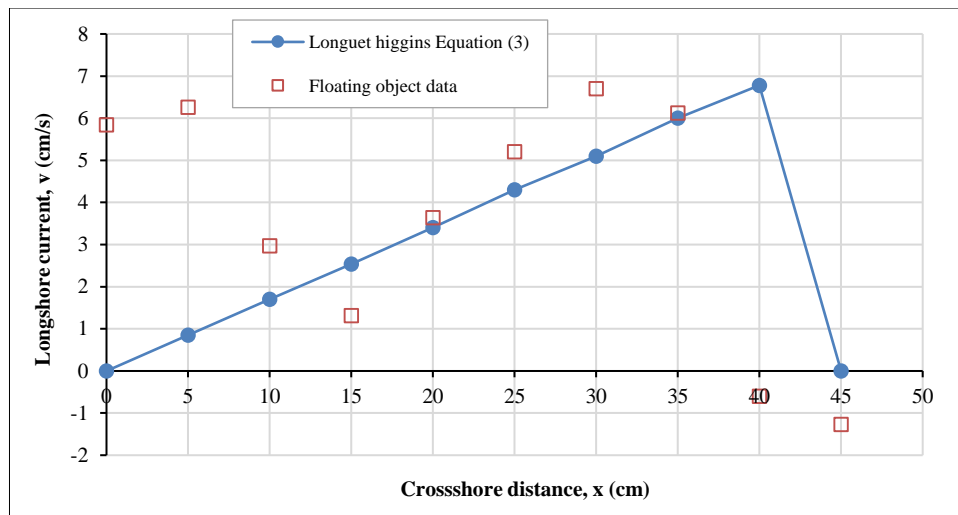


Figure 6. The results of measuring and calculating the speed of longshore currents at each point in the surf zone area under groin conditions

4. Model Development

4.1. Experimental Insights

The relationship between the empirically obtained data on current velocity along the coast and the calculations based on Equation 1 is illustrated in Figure 7, where the current velocity data v at a comparable wave height H_b aligns closely with the theoretical line. This equation is utilized with a coefficient of friction C_f set at 0.04, showcasing the correlation between breaking wave height H_b and current velocity v

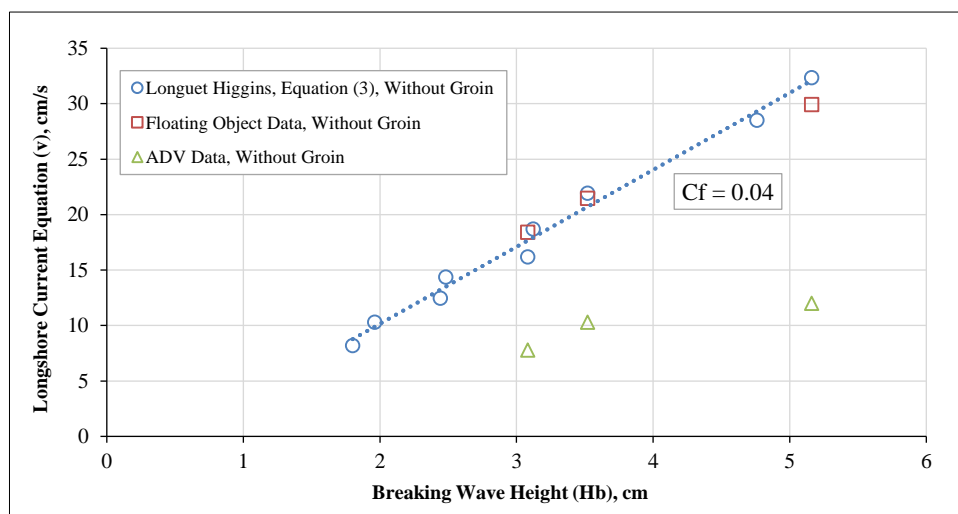


Figure 7. Relationship between breaking wave height H_b and current velocity v without groin

The findings suggest that as the wave height increases, so does the generated current, as indicated by the direct proportionality between H_b and v . Moreover, comparing the Acoustic Doppler Velocimeter (ADV) and buoy measurement results reveals discrepancies, with ADV measurements yielding smaller values. The ADV measurements and theoretical calculations based on Equation 1 are shown to be less accurate than buoy measurements and theoretical calculations, respectively. These discrepancies can be attributed to the ADV instrument's limitations, particularly its water depth sensitivity. The ADV sensor signal is only reliable for current velocity measurements when the water depth exceeds 5 cm, rendering the accuracy of ADV measurements questionable for research conditions with depths below this threshold.

Figure 8 provides a visual representation of the impact of an impermeable groin structure on the current flow. Before the presence of the groin structure, the average current velocity measured 27.94 cm/s. However, after installing the impermeable groin structure, the velocity decreased to 5.94 cm/s, significantly reducing 80.08%. It is worth noting that the wave-breaking height H_b measured 5.16 cm during the observation period. This indicates that while the impermeable groin structure does impede the occurrence of currents, it does not entirely resemble an ideal channel model. The surf zone area on the beach lacks the characteristics of a channel model that a boundary wall could entirely obstruct. Despite the groin structure covering the entire width of the surf zone, there are still currents capable of traversing the end of the groin. These findings emphasize the importance of considering friction parameters in greater detail when assessing the effectiveness of permeable groins.

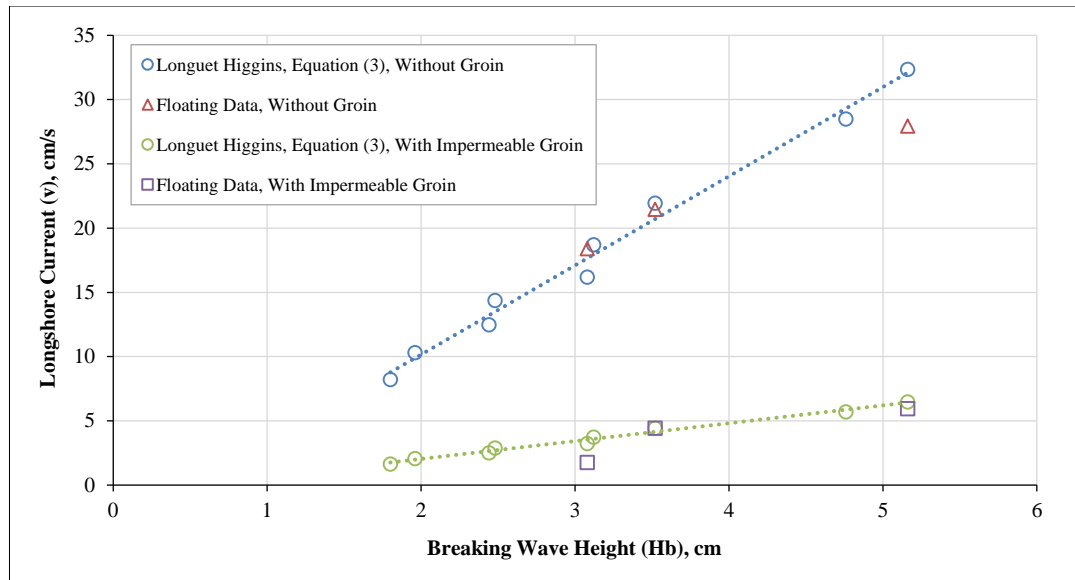


Figure 8. Relationship between breaking wave height H_b and current velocity v with impermeable groin

4.2. New Exact Solution

This research delves deep into permeable groin construction resistance, utilizing this aspect to derive a theoretical model for the longshore current equation. The novel approach involves incorporating the essential friction parameter stemming from the permeable groin into the existing empirical theory, thereby paving the way for a more comprehensive understanding of the dynamics at play. This new theoretical framework involves meticulous research to refine and enhance the long-shore current equation within permeable groin structures. These meticulously planned and executed steps are the foundation for developing a robust and insightful analytical tool that can provide valuable insights into coastal processes. By documenting each stage of the research journey and analyzing the data collected, the study aims to shed light on the intricate interplay between pile groin construction resistance and the longshore current.

At the initial stage, the base friction is assumed to be increased by the presence of the pile-permeable groin structure. So that the base shear stress after the permeable groin structure, the bed shear stress $\langle \tau_{by} \rangle_{groin}$ is thought to be equal to the bed shear stress plus the drag or friction factor produced by the permeability pile groin structure, and the equation for the momentum of the longshore direction after the pile groin structure becomes

$$\tau_y = \langle \tau_{by} \rangle_{groin} \tag{7}$$

$$\langle \tau_{by} \rangle_{groin} = \langle \tau_{by} \rangle + \langle \tau_g \rangle \tag{8}$$

where $\langle \tau_{by} \rangle_{groin}$ is the shear stress due to the permeable groin resistance, which is a function of the average bed shear stress $\langle \tau_{by} \rangle$ plus the average shear stress between the water and the groin piles $\langle \tau_g \rangle$,

The shear stress between the water and the groin piles $\langle \tau_{by} \rangle_{groin}$ is assumed to be equal to the drag force of the permeable groin structure F_d per unit area of the groin resistance area. In the research model, the groin resistance area is the length of the groin L_g multiplied by the groin width, which is the same as pile diameter d_t .

$$\langle \tau_g \rangle = \frac{F_d}{L_g d_t} \tag{9}$$

where,

$$F_d = \frac{1}{2} C_d \rho A u_m \langle v \rangle \tag{10}$$

So that the average shear stress can be written as follows,

$$\langle \tau_g \rangle = \frac{F_d}{L_g d_t} = \frac{\frac{1}{2} C_d \rho A u_m \langle v \rangle}{L_g d_t} \tag{11}$$

where $\langle \tau_g \rangle$ is the drag force; L_g is the length of the groin (m); d_t is the diameter of the groin pile (m); C_d is the drag coefficient of the groin piles; A is the area of the groin piles blocking the current (m²); u_m is the maximum orbital velocity of the wave near the bed (m/s), and $\langle v \rangle$ is the average velocity of the longshore current (m/s).

To write the equation for the average shear stress,

$$\langle \tau_g \rangle = \frac{1}{2} C_d \rho \left(\frac{N}{L_g d_t} \right) h_r d_t u_m \langle v \rangle \quad (12)$$

$$\text{Open } \langle \tau_{b_y} \rangle_g = \frac{2}{\pi} C_f \rho u_m \langle v \rangle + \frac{1}{2} C_d \rho \left(\frac{N}{L_g d_t} \right) h_r d_t u_m \langle v \rangle \quad (13)$$

where $\langle \tau_{b_y} \rangle_g$ is the shear stress due to the permeable groin resistance, C_f is friction coefficient, ρ is density (kg/m^3), u_m is the maximum orbital velocity (m/s), $\langle v \rangle$ is the average velocity of the longshore current (m/s), C_d is the drag coefficient of the groin piles, N is the number of piles, h_r is the mean height of the water surface that submerges the groin piles (m), d_t is the diameter of piles (m), $\langle v \rangle$ is longshore current (m/s).

Secondly, the groin pile arrangement volume along the groin structure V_g to the volume of water in the groin area drowning the groin piles V_a was calculated as the groin density.

$$p = \frac{V_g}{V_a} \times 100\% \quad (14)$$

$$V_g = N A h_r \quad (15)$$

If it was known that the relationship between the number of piles N , the cross-sectional area of the piles A , and the mean depth h_r affected the volume of the groin pile arrangement V_g ,

$$V_a = L_g d_t h_r V_g \quad (16)$$

$$A = \frac{\pi d_t^2}{4} \quad (17)$$

In order to write the groin density p equation as follows,

$$p = \frac{N \pi d_t^2}{4 L_g d_t} \times 100\% = \frac{N \pi d_t}{4 L_g} \times 100\% \quad (18)$$

Third, the mean depth characteristics of submerged groin structures were evaluated. The underwater pile groin's average height h_r is,

$$h_r = \frac{1}{N} \int_0^N h_n dN = \frac{1}{N} \int_0^N h - \frac{hNb}{x} + \frac{hb}{x} dN \quad (19)$$

$$h_r = \frac{1}{N} \left(hN - \frac{1}{2} \frac{hbN^2}{x} + \frac{hbN}{x} \right)$$

If $\frac{h}{x} = \tan \beta$, then, the mean height of the water surface that submerges the groin piles h_r is,

$$h_r = h - \left(\frac{N}{2} - 1 \right) \tan \beta b \quad (20)$$

where h is the depth of water (MSL), N is the number of piles; $\tan \beta$ is the slope of the coast, and b is the distance between groin piles.

Following the presence of groin structure resistance and after balancing the shear stress caused by waves τ_y with the mean bed shear $\langle \tau_{b_y} \rangle_{groin}$ stress caused by the groin pile, the momentum equation in the y -direction was used to produce the equation for the longshore current's velocity via the groin pile.

If the following wave shear stress τ_y equation:

$$\tau_y = \frac{5}{4} \rho u_m^2 \tan \beta \sin \alpha \cos \alpha \quad (21)$$

The following equation is then produced by substituting Equations 13 and 21 into Equation 7:

$$\frac{5}{4} \rho u_m^2 (\tan \beta \sin \alpha_b) = \frac{2}{\pi} C_f \rho u_m \langle v \rangle + \frac{1}{2} C_d \rho \left(\frac{N}{L_g d_t} \right) h_r d_t u_m \langle v \rangle \quad (22)$$

$$\frac{5}{4} u_m (\tan \beta \sin \alpha_b) = \left(\frac{2}{\pi} C_f + \frac{1}{2} C_d \left(\frac{N}{L_g d_t} \right) h_r d_t \right) \langle v \rangle$$

The following equation for the longshore current can be obtained through the groin:

$$\langle v \rangle_{groin} = \frac{\frac{5}{4} u_m (\tan \beta \sin \alpha_b)}{\left(\left(\frac{2}{\pi} + \frac{\gamma}{4} \right) C_f + \frac{4 C_d p h_r}{2 \pi d_t} \right)} \quad (23)$$

or;

$$\langle v \rangle_{groin} = \frac{\frac{5}{8} H_b \sqrt{\frac{g}{h_b}} (\tan \beta \sin \alpha_b)}{\left(\left(\frac{2}{\pi} + \frac{\gamma}{4} \right) C_f + \frac{4 C_d p h_r}{2 \pi d_t} \right)} \quad (24)$$

where $\langle v \rangle_{groin}$ is longshore current with groin (m/s), H_b is breaking wave height (m), γ is the ratio between the breaking wave height (H_b) and the breaking wave depth (h_b), g is gravity acceleration (m^2/s), $\tan \beta$ is beach slope, h_b is the breaking wave depth (m), α_b is breaking wave angle, C_f is friction coefficient, C_d is drag coefficient, p is groin density, h_r is the mean height of the water surface that submerges the groin piles (m), d_t is the diameter of piles (m).

Moreover, Equation 24 determines the friction coefficient C_f as 0.04 without groins. The US Army Corps of Engineers - Coastal Engineering Manual (CEM) [26] states that C_f can range from 0.05 to 1, with values exceeding one also reported. Prandtl [27] found values from 0.05 to 1, while Bretschneider [28] reported values from 0.034 to 0.097, and Miller [29] found values of 0.01 to 0.02. The analysis used a C_f of 0.04, consistent with Bretschneider [28]. The reduction in current due to permeable groin piles depends on roughness parameters such as the Chezy coefficient of roughness C_I , the coefficient of friction C_f , and the drag coefficient C_d . The reduction coefficient Equation C_r may be calculated as follows:

$$C_r = \frac{\langle v \rangle_{groin}}{\langle v \rangle_{w/o groin}} = \frac{\left(\frac{2+\gamma}{\pi+4}\right)C_f}{\left(\frac{2+\gamma}{\pi+4}\right)C_f + \frac{2C_d p h_r}{\pi d_t}} \tag{25}$$

Given the values of π and γ (3.14 and 0.78, respectively), it is possible to express Equation 25 in the following way:

$$C_r = \frac{1}{1 + \frac{C_d p h_r}{1.3 C_f d_t}} \tag{26}$$

where C_r is reduction coefficient, C_f is friction coefficient, C_d is drag coefficient, p is groin density, h_r is the mean height of the water surface that submerges the groin piles (m), d_t is the diameter of piles (m).

4.3. New Exact Validation

Creating a viable explanation for the longshore current at permeable groins and determining a significant friction coefficient is challenging. Nonetheless, it is essential to validate the efficacy of this novel theory using empirical evidence and explore its suitability in scenarios previously overlooked by current theories.

Figures 9 and 10 provide compelling evidence to support the success of the new theory. These figures depict the correlation between breaking wave height H_b and average current velocity after implementing permeable groins with varying groin densities of 54%, 51%, 47%, and 43%. By comparing Figure 8 with Figures 9 and 10, it becomes evident that the current velocity following the installation of the permeable groin structure surpasses that of the impermeable groin. This observation indicates that permeable groins do not entirely obstruct the current flow. Moreover, it is crucial to note that the new theory effectively captures this behavior, further validating its success.

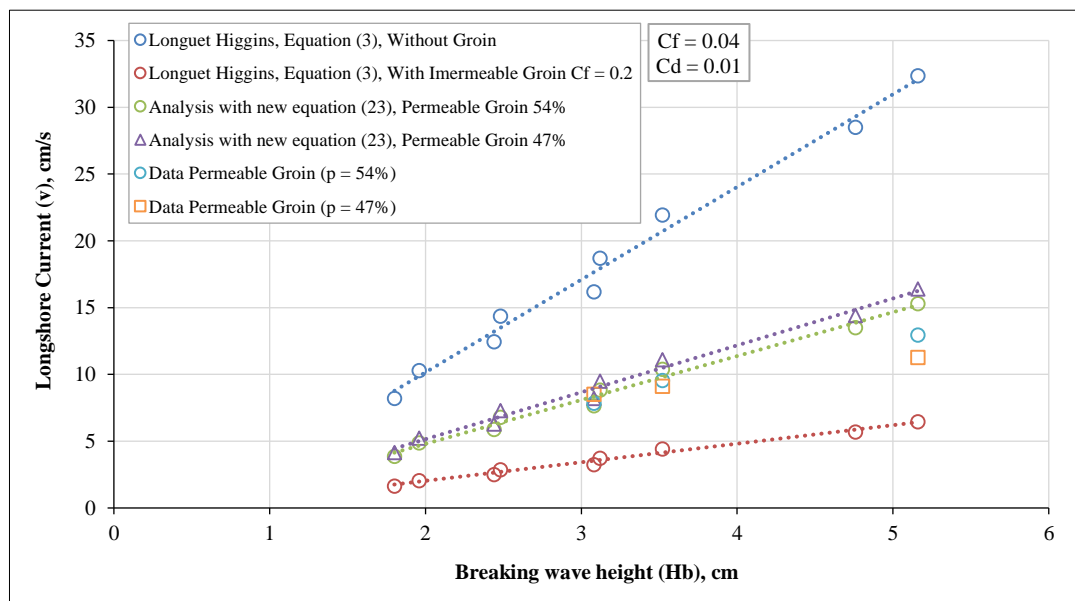


Figure 1. Relationship between breaking wave height H_b and current velocity v with groin permeability 54% and 47% for depth 1.5 cm

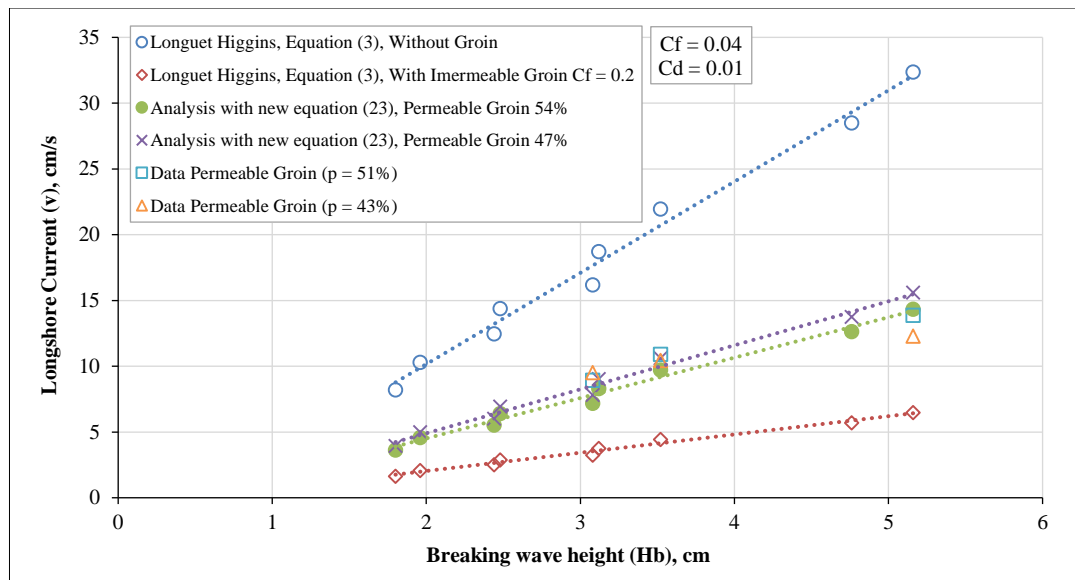


Figure 2. Relationship between breaking wave height H_b and current velocity v with groin permeability 51% and 43% for depth 1.25 cm

The down-shore current's control is directly linked to the density of groins, with a higher percentage of groin density resulting in a decreased ability of the groin structure to allow the current to pass through. This relationship is evident from Tables 2 to 5, where a decrease in mean velocity is observed with a permeable groin structure.

The data indicates that a lower groin density leads to a higher reduction coefficient in the velocity of the down-shore current. On average, the reduction in current velocity along the beach is approximately 50%, highlighting the effectiveness of the permeable groin structure in halving the current velocity compared to the absence of groin structure, as detailed in [30].

Table 2. Reducing the average current velocity with permeable groin structure by 54% ($d_t= 1.5$ cm, $a= 0.7$ cm)

Breaking wave height H_b (cm)	Longshore current without groin (cm/s)	Longshore current with groin permeable	Reduction (%)
5.16	27.94	12.95	53.65
3.52	21.47	9.55	55.50
3.08	18.40	7.84	57.40

Table 3. Reducing the average current velocity with permeable groin structure by 47% ($d_t= 1.5$ cm, $a= 1.0$ cm)

Breaking wave height H_b (cm)	Longshore current without groin (cm/s)	Longshore current with groin permeable	Reduction (%)
5.16	27.94	13.88	50.32
3.52	21.47	10.90	49.20
3.08	18.40	8.94	51.42

Table 4. Reducing the average current velocity with permeable groin structure by 51% ($d_t= 1.25$ cm, $a= 0.7$ cm)

Breaking wave height H_b (cm)	Longshore current without groin (cm/s)	Longshore current with groin permeable	Reduction (%)
5.16	27.94	11.27	59.66
3.52	21.47	9.13	57.49
3.08	18.40	8.53	53.66

Table 5. Reducing the average current velocity with permeable groin structure by 43% ($d_t= 1.25$ cm, $a= 1.0$ cm)

Breaking wave height H_b (cm)	Longshore current without groin (cm/s)	Longshore current with groin permeable	Reduction (%)
5.16	27.94	12.3	56.02
3.52	21.47	10.44	51.36
3.08	18.40	9.52	48.25

The relationship between the coastal current reduction coefficient C_r and the drag coefficient C_d can be described in Figure 11 using Equation 25. This equation considers various variations of the groin density parameter p . The analysis reveals that the reduction of the down-shore current is influenced by the groin resistance, represented by the drag coefficient C_d . If the C_d is zero, the C_r equals 1, indicating the absence of groin resistance. Furthermore, the groin density also influences the drag coefficient C_d . A smaller groin density p produces a higher C_d . Although there may be slight deviations from the proposed theory, a consensus among all cases indicates a significant improvement over the existing theory.

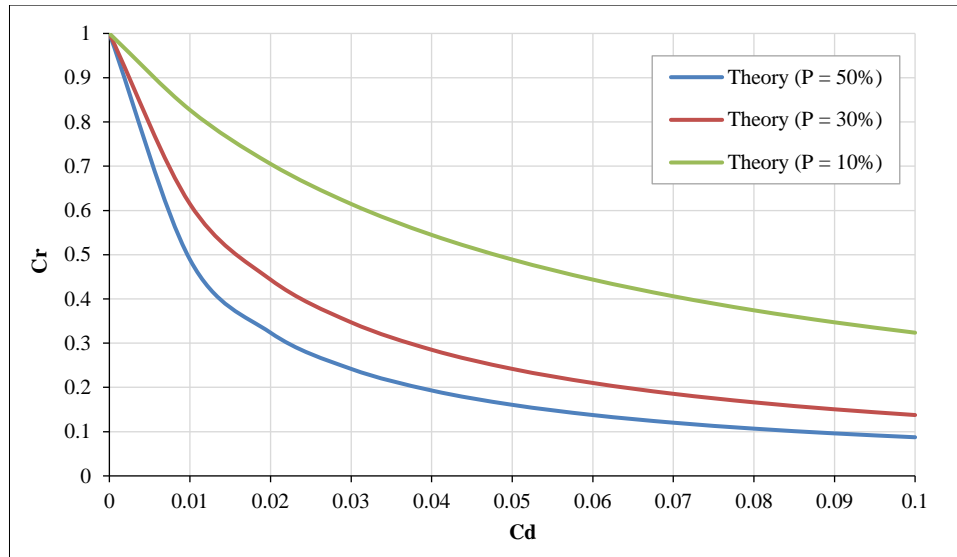


Figure 3. Relationship between reduction coefficient C_r and drag coefficient C_d

5. Conclusion

This study conducted a thorough examination to calculate longshore currents concerning permeable groins and the key factors that influence them. By gathering and analyzing a significant amount of experimental data, it has become evident that accurately determining the existence of permeable groins in terms of estimating longshore current is challenging. This can be attributed to two main factors: the average velocity of the orbital motion when considering the presence of permeable groins and the additional shear stress caused by the permeable groin.

After identifying these crucial impacts, a novel, precise solution, Equations 19 and 21, has been developed specifically for permeable groins. This theoretical framework builds upon previous research in its analytical approach and has been validated through empirical data. As a result, it fills a critical gap in the parameter space left by its predecessor.

The recent theory has demonstrated superior performance to Equation 24 in the examined scenarios. It is highlighted that the theory indicates the ability of the permeable groin structure to regulate the longshore current resulting from the groin density parameter p . As the groin density decreases, the capacity for current to flow through the groin structure increases. This observation underscores the significant impact of the drag coefficient C_d , friction coefficient C_f , and reduction coefficient C_r on longshore current reduction parameters. The comparison between the new theory and empirical data indicates a satisfactory level of agreement, utilizing a C_f of 0.04, C_d of 0.01, and γ of 0.78. The practicality of the proposed theory is emphasized as it can serve as a practical guide for the design of permeable groin structures, offering a straightforward approach to implementation.

Despite the accurate generation of longshore current in permeable groins achieved by this novel theory, it is essential to note that this is not the conclusion. Future research will delve into the impact of tidal currents on the C_d . It will also include comprehensive observations of the groin field under conditions of irregular wave generation. These aspects will contribute to a more thorough understanding of the subject matter.

6. Declarations

6.1. Author Contributions

Conceptualization, H.U., R.T., and F.M.A.; methodology, H.U. and R.T.; software, H.U. and R.T.; validation, H.U., R.T., and F.H.; formal analysis, H.U. and R.T.; investigation, H.U.; resources, H.U.; data curation, H.U.; writing—original draft preparation, H.U.; writing—review and editing, F.M.A.; visualization, F.M.A. and H.U.; supervision, R.T. and A.Y.B.; project administration, H.U. and F.M.A.; funding acquisition, H.U. All authors have read and agreed to the published version of the manuscript.

6.2. Data Availability Statement

The data presented in this study are available on request from the corresponding author.

6.3. Funding

This work is supported by Laboratory Based Education (LBE) of the Faculty of Engineering, Universitas Hasanuddin, Indonesia (12682/UN4.7.2/PM.01.01/2024). The authors would like to express their gratitude to the anonymous reviewers of this paper for their constructive comments.

6.4. Acknowledgements

The authors acknowledge using the three-dimensional wave basin and advanced support from the Hydraulics Laboratory at Universitas Gadjah Mada to carry out the experimental simulations presented here

6.5. Conflicts of Interest

The authors declare no conflict of interest.

7. References

- [1] Nguyen, L. A., Nguyen, M. H., Reynaud, A., & Simioni, M. (2024). A comparative study of residents and tourists' valuation for a heterogeneous environmental good: The case of coastal erosion. *Marine Policy*, 161, 106038. doi:10.1016/j.marpol.2024.106038.
- [2] Ma, X., Wang, C., Zhao, C., Ji, M., Zhu, J., Yang, G., & Li, C. (2024). Identification and simulation the response of storm-induced coastal erosion in the China Yellow sea. *Ocean Engineering*, 300, 117394. doi:10.1016/j.oceaneng.2024.117394.
- [3] Dong, W. S., Ismailuddin, A., Yun, L. S., Ariffin, E. H., Saengsupavanich, C., Abdul Maulud, K. N., Ramli, M. Z., Miskon, M. F., Jeofry, M. H., Mohamed, J., Mohd, F. A., Hamzah, S. B., & Yunus, K. (2024). The impact of climate change on coastal erosion in Southeast Asia and the compelling need to establish robust adaptation strategies. *Heliyon*, 10(4), 25609. doi:10.1016/j.heliyon.2024.e25609.
- [4] Deng, B., Wu, H., Yang, S., & Zhang, J. (2017). Longshore suspended sediment transport and its implications for submarine erosion off the Yangtze River Estuary. *Estuarine, Coastal and Shelf Science*, 190, 1–10. doi:10.1016/j.ecss.2017.03.015.
- [5] Jones, B. D., Collings, B., Dickson, M. E., Ford, M., Hikuroa, D., Bickler, S. H., & Ryan, E. (2024). Regional implementation of coastal erosion hazard zones for archaeological applications. *Journal of Cultural Heritage*, 67, 430–442. doi:10.1016/j.culher.2024.04.007.
- [6] Dal Barco, M. K., Furlan, E., Pham, H. V., Torresan, S., Zachopoulos, K., Kokkos, N., Sylaios, G., & Critto, A. (2024). Multi-scenario analysis in the Apulia shoreline: A multi-tiers analytical framework for the combined evaluation and management of coastal erosion and water quality risks. *Environmental Science and Policy*, 153, 103665. doi:10.1016/j.envsci.2023.103665.
- [7] Mensah, J., & Mattah, P. A. D. (2023). Illegal sand mining in coastal Ghana: The drivers and the way forward. *Extractive Industries and Society*, 13, 101224. doi:10.1016/j.exis.2023.101224.
- [8] Lubis, A. M., Veronica, N., Saputra, R., Sinaga, J., Hasanudin, M., & Kusmanto, E. (2020). Investigasi Arus Sejajar Pantai (Longshore Current) di Daerah Abrasi Bengkulu Utara. *Jurnal Kelautan Tropis*, 23(3), 316–324. doi:10.14710/jkt.v23i3.8045.
- [9] Hamid, N., Setyowati, D. L., Juhadi, Priyanto, A. S., Hardati, P., Soleh, M., Wijayanti, N. R., & Aroyandini, E. N. (2021). The Effect of Human Activities Towards Coastal Dynamics and Sustainable Coastal Management. *International Journal of Sustainable Development and Planning*, 16(8), 1479–1493. doi:10.18280/ijstdp.160809.
- [10] Vaidya, A. M., Kori, S. K., & Kudale, M. D. (2015). Shoreline Response to Coastal Structures. *Aquatic Procedia*, 4, 333–340. doi:10.1016/j.aqpro.2015.02.045.
- [11] Guimarães, A., Lima, M., Coelho, C., Silva, R., & Veloso-Gomes, F. (2016). Groin impacts on updrift morphology: Physical and numerical study. *Coastal Engineering*, 109, 63–75. doi:10.1016/j.coastaleng.2015.12.003.
- [12] Lima, M., Coelho, C., Veloso-Gomes, F., & Roebeling, P. (2020). An integrated physical and cost-benefit approach to assess groins as a coastal erosion mitigation strategy. *Coastal Engineering*, 156, 103614. doi:10.1016/j.coastaleng.2019.103614.
- [13] Saengsupavanich, C., Rif'atin, H. Q., Magdalena, I., & Ariffin, E. H. (2024). A systematic review of jetty-induced downdrift coastal erosion management. *Regional Studies in Marine Science*, 74, 103523. doi:10.1016/j.risma.2024.103523.
- [14] Shi, L., Liu, W., Zhou, C., & Cai, Y. (2024). A structure-decomposition approach for dynamic analysis of sheet-pile groins subjected to tidal bores. *Ocean Engineering*, 299, 117322. doi:10.1016/j.oceaneng.2024.117322.

- [15] Shokrian Hajibehzad, M., Shafai Bejestan, M., Ferro, V., & Avarand, R. (2022). Mean flow, secondary currents and bed shear stress at a 180-degree laboratory bend with and without enhanced permeable groins as an Eco-friendly river structure. *Journal of Hydro-Environment Research*, 44, 12–22. doi:10.1016/j.jher.2022.07.004.
- [16] Wu, T., Zhang, Y., Sun, H., Galindo, R., Wu, W., & Cai, Y. (2023). Dynamic response of sheet–pile groin under tidal bore considering pile–pile mutual interaction and hydrodynamic pressure. *Soil Dynamics and Earthquake Engineering*, 164, 107568. doi:10.1016/j.soildyn.2022.107568.
- [17] Zhang, R., & Stive, M. J. F. (2019). Numerical modelling of hydrodynamics of permeable pile groins using SWASH. *Coastal Engineering*, 153, 103558. doi:10.1016/j.coastaleng.2019.103558.
- [18] Heikal, E. M., Koraim, A. S., Rafea, A. A., & Elbagory, I. A. (2023). The effect of groins characteristic on sandy beach stability. *Egyptian Journal of Aquatic Research*, 49(3), 303–312. doi:10.1016/j.ejar.2023.04.005.
- [19] Abdel-Mawla, S., & Khaled, M. (2002). Application of Permeable Groins on Tourist Shore Protection. *Ocean Wave Measurement and Analysis* (2001), 1735–1744. doi:10.1061/40604(273)175.
- [20] Longuet-Higgins, M. S. (1970). Longshore currents generated by obliquely incident sea waves: 1. *Journal of Geophysical Research*, 75(33), 6778–6789. doi:10.1029/jc075i033p06778.
- [21] Longuet-Higgins, M. S., & Stewart, R. w. (1964). Radiation stresses in water waves; a physical discussion, with applications. *Deep-Sea Research and Oceanographic Abstracts*, 11(4), 529–562. doi:10.1016/0011-7471(64)90001-4.
- [22] Triatmodjo, B. (1999). *Coastal Engineering*. Penerbit Beta Offset, Yogyakarta, Indonesia. (In Indonesian).
- [23] Meilistya, R.R.I., Sugianto, D.N., & Indrayanti, E. (2012). Longshore Current Study Due to the Influence of Wave Transformation in Semarang Waters. *Jurnal Oseanografi*, 1(2), 128-138.
- [24] Komar, P. D., & Inman, D. L. (1970). Longshore sand transport on beaches. *Journal of Geophysical Research*, 75(30), 5914–5927. doi:10.1029/jc075i030p05914.
- [25] Larson, M., & Kraus, N. C. (1991). Numerical Model of Longshore Current for Bar and Trough Beaches. *Journal of Waterway, Port, Coastal, and Ocean Engineering*, 117(4), 326–347. doi:10.1061/(asce)0733-950x(1991)117:4(326).
- [26] Sabatier, F. (2007). U.S. Army Corps of Engineers, Coastal Engineering Manual (CEM), Engineer Manual 1110-2-1100. *Méditerranée*, 108, 146. doi:10.4000/mediterranee.201.
- [27] Prandtl, L. (1952). *Essentials of fluid dynamics with applications to hydraulics, aeronautics, meteorology and other subjects*. Hafner Publishing Company, New York, United States.
- [28] Bretschneider, C. L. (1954). Field investigations of wave energy loss in shallow water ocean waves. Beach Erosion Board, Engineer Research and Development Center, Vicksburg, United States.
- [29] Miller, R. L. (1968). Experimental determination of run-up of undular and fully developed bores. *Journal of Geophysical Research*, 73(14), 4497–4510. doi:10.1029/jb073i014p04497.
- [30] Raudkivi, A. J. (1996). Permeable Pile Groins. *Journal of Waterway, Port, Coastal, and Ocean Engineering*, 122(6), 267–272. doi:10.1061/(asce)0733-950x(1996)122:6(267).